Deployment of POLARBEAR-2b

**Megan Russell[1] · Kana Sakaguri[2] · Lindsay Ng Lowry[3] · Tylor Adkins[3] ·
Kam Arnold[1] · Carlo Baccigalupi[8,9,10] · Kevin T. Crowley[1] · Tucker Elleflot[5] ·
Nicole Farias[3] · Masashi Hazumi[6] · Jennifer Ito[7] · Oliver Jeong[3] · Adrian Lee[3,5] ·
Michael Lew[7] · Jacob Nelson[7] · Praween Siritanasak[4] · Tran Tsan[1] ·
the POLARBEAR Collaboration**

Abstract

POLARBEAR-2b (PB-2b) is the second receiver in the Simons Array, a cosmic microwave background (CMB) polarization experiment. The Simons Array uses dichroic polarization sensitive lenslet-coupled sinuous antennas and transition-edge sensor (TES) bolometers made of superconducting films. These bolometers are read out with frequency multiplexing electronics. PB-2b contains ~ 7500 detectors in two bands at 90 and 150 GHz with arcminute resolution. The polarization of these detectors is modulated by a cryogenic continuously rotating half-wave plate. PB-2b was installed on its telescope in 2022 in the Atacama Desert at an altitude of 5.2 km. This paper will detail initial readout commissioning, test of a new loopgain monitoring method, and focusing the optics. Work is ongoing to commission the remaining ambient temperature readout electronics, measure detector time constants, and observe with the cryogenic half-wave plate spinning

Kana Sakaguri and Lindsay Ng Lowry have equally contributed to this work.

✉ Megan Russell
mer044@ucsd.edu

1   University of California, San Diego, La Jolla, CA, USA

2   The University of Tokyo, Tokyo, Japan

3   University of California, Berkeley, Berkeley, CA, USA

4   National Astronomical Research Institute of Thailand, Chiangmai, Thailand

5   Lawrence Berkeley National Laboratory, Berkeley, CA, USA

6   International Center for Quantum-field Measurement Systems for Studies of the Universe and Particles (QUP), High Energy Accelerator Research Organization (KEK), Tsukuba, Japan

7   Westmont College, Santa Barbara, CA, USA

8   International School for Advanced Studies (SISSA), Trieste, Italy

9   Institute for Fundamental Physics of the Universe (IFPU), Trieste, Italy

10   National Institute for Nuclear Physics (INFN), Trieste, Italy
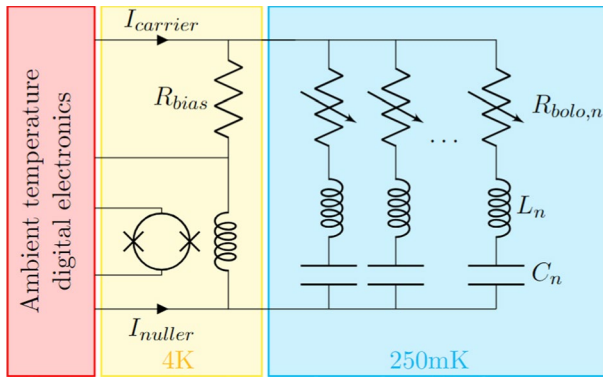
Ⓐ Springer

Fig. 1 This circuit diagram shows the readout scheme used by PB-2b [2]. Each bolometer is represented by a variable resistor and is in series with a superconducting LC resonator, which determines the frequency of the AC voltage bias supplied to the bolometer. Each superconducting LC resonator is referred to as a channel. The bias current and any current from optical signal are canceled out with digital active nulling [4], before the remaining current is amplified by a DC SQUID array operating as a transimpedance amplifier

Keywords CMB · Millimeter wave · TES bolometer · FDM readout

1 Introduction

POLARBEAR-2b (PB-2b) is the second receiver in the Simons Array, a cosmic microwave background (CMB) polarization experiment [1]. PB-2b was installed on its telescope in 2022 in the Atacama Desert at an altitude of 5.2 km. The telescope has a 3.5 m primary and detectors with arcminute resolution. Of the 7500 detectors, 2072 have so far been calibrated with planet observations. The readout system used is digital frequency multiplexing electronics (DfMUX) [2]. This paper will cover early results from the commissioning of the readout electronics, focusing of the optics, and preliminary tests of bolometer performance.

2 Readout Performance

A circuit diagram showing the DfMUX implementation used in PB-2b is shown in Fig. 1. In this circuit, bolometers are biased with MHz tones, and the currents flowing through them are amplified by a superconducting quantum interference devices (SQUIDs) operating as a cryogenic transimpedance amplifier. Ambient temperature electronics amplify the signal further, filter the output to minimize aliasing, and digitize the signal [3].

Since the installation of the receiver, about 75% of the DfMUX readout electronics have been commissioned. The remainder of the readout will be commissioned after the installation of the remaining ambient temperature electronics.

Commissioning that portion of the readout has shown that 55% of the *LC* resonators have failed to yield. This component could be replaced in a retrofit.

The SQUIDs, which act as cryogenic amplifiers, lower the noise of ambient temperature readout electronics when noise is referred to the input coil of the SQUID. The output impedance of the SQUID has a smaller impact on the readout noise but can increase the noise of channels at high bias frequencies when it is large enough to create a low pass filter with the parasitic capacitance of the wiring harness [5, 6]. The deployed SQUIDs have a median transimpedance of 730Ω, with 95% of SQUIDs achieving a transimpedance greater than 500 Ω. The output impedance of the SQUIDs has a median of 715 Ω, with 99% lower than 1000 Ω. This performance is acceptable and improved somewhat from last laboratory tests of PB-2b [7]. The median readout noise is 19 pA/$\sqrt{\text{Hz}}$, with some dependence on the MHz frequency, the bolometer is biased at. This noise level is similar to what was measured in laboratory tests as well [8]. A histogram of these data can be found in Fig. 2. In this figure, data for 2133 channels are presented. These data were taken while the bath temperature was greater than the critical temperature, $T_c \approx 450$ mK, of the TES so that photon and phonon noise does not contribute to this measurement. However, the readout noise may also change when the TES is operating at lower impedances in the transition, as they do during observation. During operation, we expect the Johnson noise of the TES to be suppressed by its loopgain, and the current sharing factor to be increased. Loopgain will be discussed further in Sect. 3. Current sharing is a factor which depends on the operating resistance of the bolometers and will increase the readout noise of detectors operated at a high bias frequency [5, 6, 9]. The net effect on the readout noise will be measured, but the change is expected to raise the median noise by less than 1pA/$\sqrt{\text{Hz}}$.

With bath temperatures greater than T_c, the median total resistance in series with the LC resonators is 1.1 Ω. These data are shown in Fig. 3, with TES resistance, and stray resistance in series with the TES separated. Work is ongoing to connect and
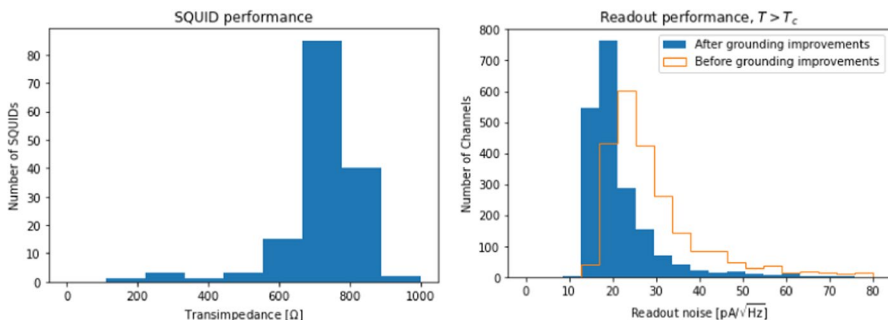

Fig. 2 Left: Histogram of the achieved transimpedance of the SQUIDs currently being operated. Right: Histogram of the readout noise measured when TES is above their critical temperature. Readout noise data are shown before and after changes to grounding improved the noise. These changes to grounding included reducing the interference from noisy electronics on the telescope, such as the motors driving it, by changing the cryostat's ground connection. Additionally as described in Montgomery et al. [5], the resistor between the negative side of the nuller line and ground was increased to 100 Ω to reduce the effects of current sharing
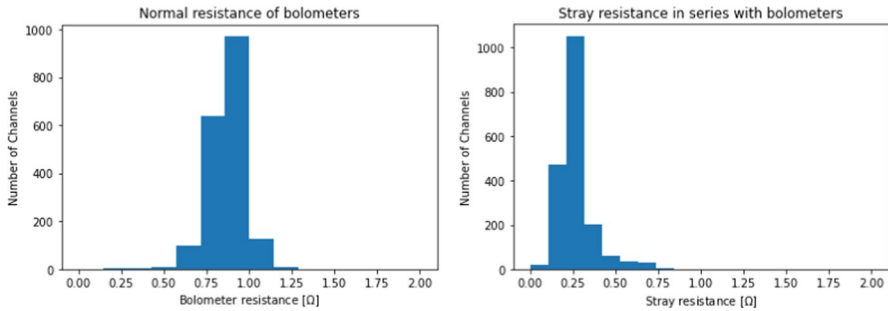
Fig. 3 Left: Histogram of measured bolometer normal resistance, excluding stray resistance. Right: Histogram of measured stray resistance while bolometers are superconducting

operate more readout electronics in the coming months. See Ito et al. [7] for details on measurements taken in the laboratory.

3 Bolometer Performance

Bolometer performance is being evaluated and their operation optimized. In addition to estimating the noise equivalent temperature of a detector from planet observations, we are using a new method to monitor the loopgain of detectors in the transition. The detector loopgain is a measure of the strength of the electrothermal feedback [10], and achieving a loopgain greater than 10 lowers the readout contribution to the noise equivalent temperature of the detector. This technique applies a small additional voltage bias offset from the channel's resonance frequency into the detector sideband. As the loopgain increases, this injected signal is suppressed, and a negative sideband is created by electrothermal feedback. This technique is explained in more detail in De Haan et al. [11]. This is being used to measure how loopgain changes with respect to the fractional resistance, $R_{\text{frac}} = R_{\text{operating}}/R_{\text{normal}}$, the bolometer is being operated at. Examples of a single bolometer's response at four different fractional resistances along with the measured loopgain associated with it are shown in Fig. 4. This figure shows that the bolometer has achieved a loopgain greater than 6 at an R_{frac} of 0.85.

4 Calibration Observations

Observations of astronomical sources are being used to measure the detector beam size, to determine the pointing offset from boresight, and to calibrate the gain of the detector. Here, data from observations of Jupiter are shown. The detector's response is filtered to remove atmospheric effects and fit to a two-dimensional elliptical Gaussian, which give the beam size, offset, and amplitude of response. An example
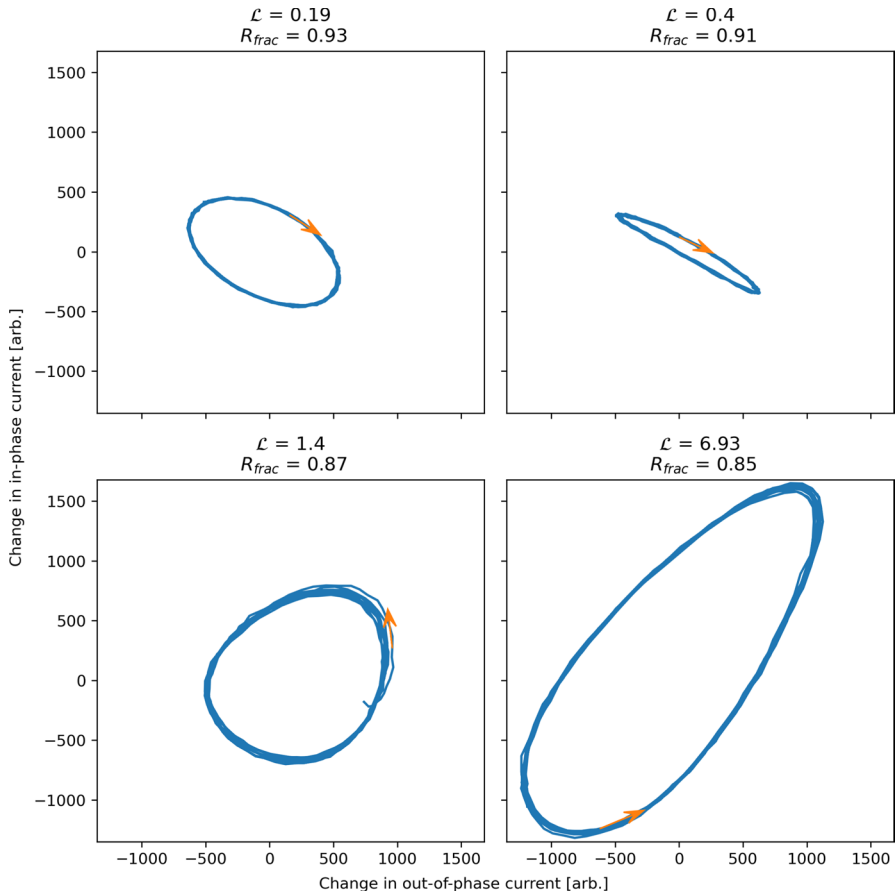
Fig. 4 Example bolometer response to small additional voltage bias, at a range of fractional resistances. As the bolometer is operated at lower fractional resistances, the measured loopgain increases. Orange arrows are plotted on top of the data to indicate the direction of rotation of the bolometer's response

of a single detector's observation of Jupiter and the beam offsets for the detectors currently being operated are shown in Fig. 5.

After the receiver was installed on the telescope, the positioning had to be fine tuned to achieve properly focused beams. This was achieved by moving the receiver along the optical axis. At each receiver position, planets were observed to determine the full-width at half-max (FWHM) of the beam. These data were then used to choose the final receiver position. This minimization was done by fitting FWHM versus receiver position to a Gaussian beam profile for 90 and 150 GHz separately, as well as the FWHM in azimuth and elevation separately. Figure 6 shows these data, as well as a comparison of the beam sizes before and after this optimization. Ultimately, only the 150 GHz fits were used to choose the final position, due to the much lower sensitivity of the 90 GHz beams to the
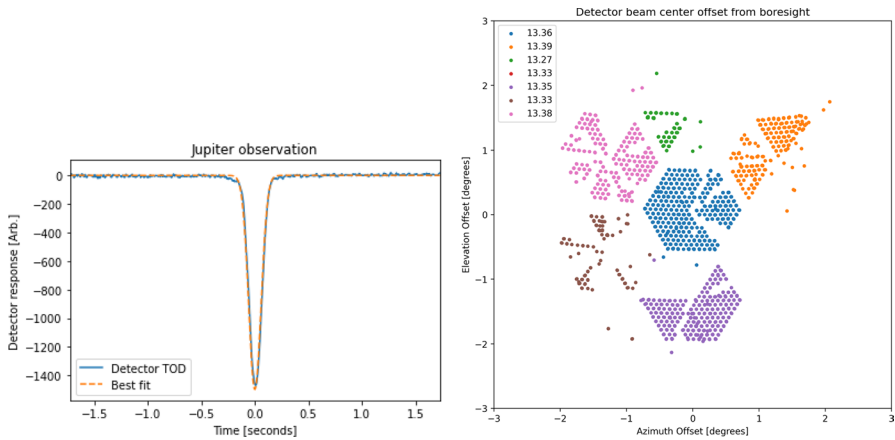
Fig. 5 Left: Example filtered bolometer response from a Jupiter observation and resulting fit of a two-dimensional elliptical gaussian. During observation, a raster scan was performed, and each detector passed over Jupiter several times at a range of elevation offsets. Shown is a single scan at constant elevation. Right: Median detector offset from all observations performed during receiver focusing. In this figure, data for 2072 channels, the number of optically active bolometers for which we have measured beams above a threshold precision, are presented. Marker color indicates detectors from different wafers of detectors [12]
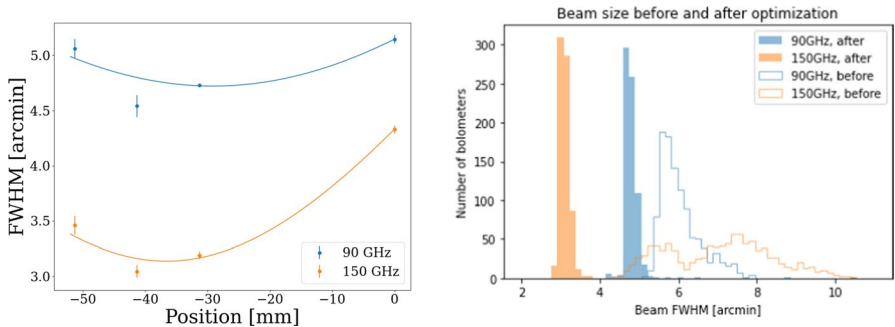
Fig. 6 Left: Beam FWHM in the azimuth direction at a range of receiver positions, obtained from gaussian beam fits. These FWHM were fit to a Gaussian beam profile used to determine optimal receiver position. Right: Histogram of beam FWHM at the initial and final receiver positions

receiver position. The minima were found to be −33.4 mm and −36.6 mm in the azimuth and elevation directions, and final position was chosen to be −35.0 mm. There may be room for improvement if we use data points except position 0, which is somewhat far from the focus position.

At the final receiver position, the mean beam FWHM was 4.79 ± 0.13 arcminutes at 90 GHz and 3.10 ± 0.12 arcminutes at 150 GHz, and the design value is 5.2 arcminutes and 3.5 arcminutes [13]. Thus, they achieve beam size better than design values. We note that the design values are not based on optics simulations and do not reflect details such as the detector beam. Thus, the measured
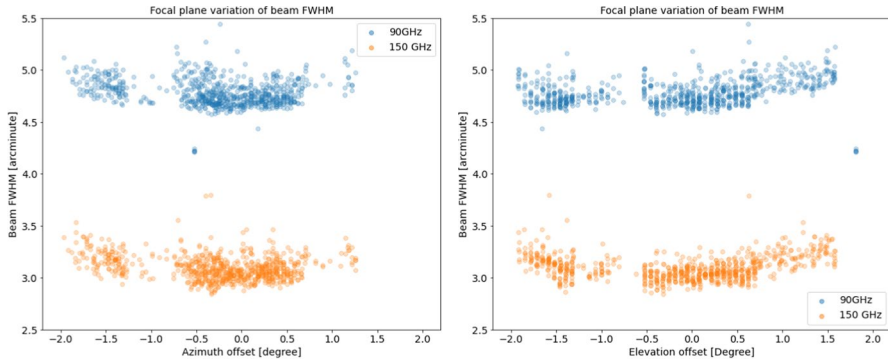
Fig. 7 Both plots show the variation of beam FWHM as a function of detector's beam center offset from boresight. Left: FWHM variation versus offset in azimuth. Right: FWHM variation versus offset in elevation

values and the design values are not directly comparable, e.g., to calculate the Strehl ratio. The relatively small variation of the beam size across the focal plane is shown in Fig. 7.

5 Conclusion

Early results show the ability to read out a large fraction of the available channels, with work ongoing to connect the remaining warm readout electronics. Observations of calibration sources are being used to evaluate detector beams and noise equivalent temperatures. The focus of the telescope has been optimized, and beam sizes across the focal plane have been characterized. A new method of quickly measuring detector loopgain is being used to evaluate detector performance. Operation of the cryogenic half-wave plate has been verified, although this is beyond the scope of this paper. Future work will include commissioning the remaining ambient temperature readout electronics to operate all available detectors, observations of a chopped thermal source to measure detector time constants, and observations with the cryogenic half-wave plate spinning.

Declarations

Conflict of interest The authors declare no Conflict of interest.

References

1. A. Suzuki, P. Ade, Y. Akiba, C. Aleman, K. Arnold, C. Baccigalupi, B. Barch, D. Barron, A. Bender, D. Boettger, J. Borrill, S. Chapman, Y. Chinone, A. Cukierman, M. Dobbs, A. Ducout, R. Dunner, T. Elleflot, J. Errard, G. Fabbian, S. Feeney, C. Feng, T. Fujino, G. Fuller, A. Gilbert, N. Goeckner-Wald, J. Groh, T.D. Haan, G. Hall, N. Halverson, T. Hamada, M. Hasegawa, K. Hattori, M. Hazumi, C. Hill, W. Holzapfel, Y. Hori, L. Howe, Y. Inoue, F. Irie, G. Jaehnig, A. Jaffe, O. Jeong, N. Katayama, J. Kaufman, K. Kazemzadeh, B. Keating, Z. Kermish, R. Keskitalo, T. Kisner, A. Kusaka, M.L. Jeune, A. Lee, D. Leon, E. Linder, L. Lowry, F. Matsuda, T. Matsumura, N. Miller, K. Mizukami, J. Montgomery, M. Navaroli, H. Nishino, J. Peloton, D. Poletti, G. Puglisi, G. Rebeiz, C. Raum, C. Reichardt, P. Richards, C. Ross, K. Rotermund, Y. Segawa, B. Sherwin, I. Shirley, P. Siritanasak, N. Stebor, R. Stompor, J. Suzuki, O. Tajima, S. Takada, S. Takakura, S. Takatori, A. Tikhomirov, T. Tomaru, B. Westbrook, N. Whitehorn, T. Yamashita, A. Zahn, O. Zahn, The Polarbear-2 and the Simons Array Experiments. J. Low Temp. Phys. **184**(3–4), 805–810 (2016)
2. ...D. Barron, K. Mitchell, J. Groh, K. Arnold, T. Elleflot, L. Howe, J. Ito, A.T. Lee, L.N. Lowry, A. Anderson, J. Avva, T. Adkins, C. Baccigalupi, K. Cheung, Y. Chinone, O. Jeong, N. Katayama, B. Keating, J. Montgomery, H. Nishino, C. Raum, P. Siritanasak, A. Suzuki, S. Takatori, C. Tsai, B. Westbrook, Y. Zhou, Integrated electrical properties of the frequency multiplexed cryogenic readout system for polarbear/simons array. IEEE Trans. Appl. Supercond. **31**(5), 1–5 (2021)
3. G. Smecher, F. Aubin, E. Bissonnette, M. Dobbs, P. Hyland, K. MacDermid, A biasing and demodulation system for kilopixel tes bolometer arrays. IEEE Trans. Instrum. Meas. **61**(1), 251–260 (2012)
4. T. Haan, G. Smecher, M. Dobbs, Improved performance of TES bolometers using digital feedback (2012)
5. J. Montgomery, A.J. Anderson, J.S. Avva, A.N. Bender, M.A. Dobbs, D. Dutcher, T. Elleflot, A. Foster, J.C. Groh, W.L. Holzapfel, D. Howe, N. Huang, A.E. Lowitz, G.I. Noble, Z. Pan, A. Rahlin, D. Riebel, G. Smecher, A. Suzuki, Whitehorn, N., Performance and characterization of the SPT-3G digital frequency multiplexed readout system using an improved noise and crosstalk model (2020)
6. M. Russell, K. Arnold, T. Elleflot, T. Haan, J. Hubmayr, G. Jaehnig, A. Lee, J. Montgomery, Suzuki, A., Development of frequency domain multiplexing readout using sub-kelvin SQUIDs for LiteBIRD (2022)
7. J. Ito, L.N. Lowry, T. Elleflot, K.T. Crowley, L. Howe, P. Siritanasak, T. Adkins, K. Arnold, C. Baccigalupi, D. Barron, B. Bixler, Y. Chinone, J. Groh, M. Hazumi, C.A. Hill, O. Jeong, B. Keating, A. Kusaka, A.T. Lee, K. Mitchell, M. Navaroli, A.T.P. Pham, C. Raum, C.L. Reichardt, T.J. Sasse, J. Seibert, A. Suzuki, S. Takakura, G.P. Teply, C. Tsai, Westbrook, B., Detector and readout characterization for POLARBEAR-2b (2020)

8. Lowry, L.N.: Preparation and deployment of the telescopes and POLARBEAR-2b receiver for the simons array cosmic microwave background polarization experiment. PhD thesis, University of California, San Diego (2021)

9. ...M. Abitbol, A.M. Aboobaker, P. Ade, D. Araujo, F. Aubin, C. Baccigalupi, C. Bao, D. Chapman, J. Didier, M. Dobbs, S.M. Feeney, C. Geach, W. Grainger, S. Hanany, K. Helson, S. Hillbrand, G. Hilton, J. Hubmayr, K. Irwin, A. Jaffe, B. Johnson, T. Jones, J. Klein, A. Korotkov, A. Lee, L. Levinson, M. Limon, K. MacDermid, A.D. Miller, M. Milligan, K. Raach, B. Reichborn-Kjennerud, C. Reintsema, I. Sagiv, G. Smecher, G.S. Tucker, B. Westbrook, K. Young, K. Zilic, The EBEX balloon-borne experiment-detectors and readout. Astrophys. J. Suppl. Ser. **239**(1), 8 (2018)

10. K.D. Irwin, G. C. Hilton, Transition-Edge Sensors. Topics in Applied Physics, pp. 63–150. Springer, Berlin Heidelberg (2005)

11. T. de Haan, T. Adkins, M. Hazumi, D. Kaneko, J. Montgomery, G. Smecher, Y. Zhou, Monitoring TES loop gain in frequency-domain multiplexed readout. J. Low Temper. Phys. (2023)

12. T. Tomaru, M. Hazumi, A.T. Lee, P. Ade, K. Arnold, D. Barron, J. Borrill, S. Chapman, Y. Chinone, M. Dobbs, J. Errard, G. Fabbian, A. Ghribi, W. Grainger, N. Halverson, M. Hasegawa, K. Hattori, W.L. Holzapfel, Y. Inoue, S. Ishii, Y. Kaneko, B. Keating, Z. Kermish, N. Kimura, T. Kisner, W. Kranz, F. Matsuda, T.Matsumura, H. Morii, M.J. Myers, H. Nishino, T. Okamura, E. Quealy, C.L. Reichardt, P.L. Richards, D. Rosen, C. Ross, A. Shimizu, M. Sholl, P. Siritanasak, P. Smith, N. Stebor, R. Stompor, A. Suzuki, J.-i. Suzuki, S. Takada, K.-i. Tanaka, O. Zahn, The POLARBEAR-2 experiment (2012)

13. F.T. Matsuda, Cosmic Microwave Background Polarization Science and Optical Design of the POLARBEAR and Simons Array Experiments. PhD thesis, University of California, San Diego (2017)